J Sol-Gel Sci Technol (2015) 73:417–427
DOI 10.1007/s10971-014-3551-x

ORIGINAL PAPER

Synthesis of sol–gel SiO_2-based materials using alkoxydisilane precursors: mechanisms and luminescence studies

César Fernández-Sánchez · José Antonio Rodríguez · Carlos Domínguez

Received: 11 July 2014 / Accepted: 16 October 2014 / Published online: 5 November 2014

Abstract This work reports on the mechanisms behind the sol–gel synthesis and versatile luminescent behavior of sol–gel silica-based materials based on hexamethoxydisilane (Hexamet) or hexaethoxydisilane (Hexaet) innocuous monomers, at different annealing temperatures. The resulting as-synthesized materials exhibit an intense photoluminescence (PL) band in the blue region of the spectrum, whose maximum shifted in the region of 430–650 nm by applying an annealing process at different temperatures in the range of 350–1,000 °C. This behavior could be attributed to the presence of different silica matrix defect-related luminescent mechanisms. PL emission bands of the Hexamet-derived materials prepared at higher T up to 1,300 °C slightly shifted and appeared in the region of 400–700 nm. However, those Hexaet-derived materials annealed at T between 1,000–1,150 °C showed bands peaking at and above 800 nm, these being related to a quantum confinement effect induced by the presence of silicon nanocrystals (Si_nc) within the polymer matrix. Based on studies carried out by different microscopy and chemical analysis techniques, the origin of the PL behavior was attributed to the kinetics of the hydrolysis and condensation reactions being different for each monomer, which generate different intermediates and eventual structures during the annealing process. The superior tunable luminescent performance of these environmentally-friendly materials provides them with the potential for the fabrication of silicon-based light sources.

Keywords Sol–gel silicon oxide · Alkoxydisilane · Silicon nanocrystal · Photoluminescence

C. Fernández-Sánchez (✉) · C. Domínguez
Instituto de Microelectrónica de Barcelona, Centro Nacional de Microelectrónica, Consejo Superior de Investigaciones Científicas, Campus Universitat Autónoma de Barcelona, 08193 Bellaterra, Barcelona, Spain
e-mail: cesar.fernandez@csic.es

C. Domínguez
e-mail: carlos.dominguez@imb-cnm.csic.es

J. A. Rodríguez
Instituto Superior Politécnico de Tecnologia e Ciências (ISPTEC), Avenida Luanda Sul, Rua Lateral Via S10, Talatona, Belas, Luanda, Angola
e-mail: Jose.Perez@isptec.co.ao

1 Introduction

Even though the luminescent properties of silicon oxide (SiO_2) have been known for decades, it was not really after the discovery of room temperature visible photoluminescence from porous silicon [1], that countless studies, focused on silicon-based light-emitting materials, have been published worldwide [2–8]. The efforts have been directed to incorporate optoelectronic capabilities to the mature and well developed microelectronic technology. Different mechanisms have been used to explain the observed luminescent behaviors, ranging from simple silicon oxide matrix radiative defects [9, 10], quantum confinement in silicon nanostructures (nanocrystals or nanoclusters, Si_nc here after) embedded in the silicon oxide matrix [11, 12], excitonic states localized in the interface between Si_nc and the oxide matrix [13, 14], and the presence of certain silicon related compounds [15, 16]. However, an absolute correspondence of the different proposed models with all of the observed experimental results has not been reached so far.

Sol–gel technology includes simple, versatile, advantageous and well-studied synthetic processes for material

fabrication, being extensively documented for silica-glass production [17]. Sol–gel technology has shown the potential for obtaining SiO_2 and Si_nc/SiO_2 nanocomposite materials in the form of thin films as well as in bulk structures of any required shape with the adequate structural and optical properties for the fabrication of light sources. In particular, several works have reported on the synthesis of sol–gel based materials with in situ (bulk [18] and thin film [19] configurations) and ex situ [20, 21] formation of Si_nc. However, some important drawbacks have been identified, such as the use of hazardous chemical precursors, like the traditional triethoxysilane (TREOS) showing a flash point of 10 °C, and the complexity of the technological process, respectively.

Our group is engaged in the systematic development and study of silica-based luminescent materials, obtained by sol–gel processing of two innocuous alkoxydisilanes, that is hexaethoxydisilane and hexamethoxydisilane. Both precursors are stable at room temperature and can be easily manipulated under usual laboratory conditions. Our aim is to obtain either a silicon excess for the further segregation of Si_nc through a thermal annealing, or the presence of oxygen defect (radiative) centers in as-synthesized materials, since both chemical precursors have a silicon–silicon bond in their structural units. In a previous work [22], we reported about the synthesis of three sets of bulk materials by using the two above mentioned precursors and their mixtures, as well as the observation of important differences in their luminescent behaviors, especially after thermal treatments in an inert atmosphere in the temperature range of 950–1,150 °C. It was firmly established by Raman Spectroscopy and by Time-Resolved Photoluminescence (TR-PL) Spectroscopy that the luminescence of materials prepared with hexaethoxydisilane, annealed in the mentioned T range, is due to a quantum confinement effect taking place in the Si_nc segregated during annealing. However, no formation of nanocrystals occurs during the synthesis of materials with hexamethoxydisilane and their luminescence should be associated to oxide matrix defect radiative centers. In the present work, the attention is paid to explain such radically different behavior after the annealing process of both types of materials on the basis of differences in the kinetics of the hydrolysis and condensation reactions taking place during the polymer formation of both precursors. A wider range of annealing T was explored, from 350 to 1,300 °C. Structural and optical properties of the obtained materials are analyzed by spectral photoluminescence, Fourier transform infrared spectroscopy (FTIR), X-ray photoelectron spectroscopy (XPS), high resolution transmission electron microscopy (HRTEM) and elemental chemical analysis techniques. From these studies, we pretend to elucidate the mechanisms that govern the material syntheses and their luminescent behavior according to data reported in the literature.

2 Experimental

2.1 Synthesis of the SiO_2-based materials

Hexaethoxydisilane ($C_{12}H_{30}O_6Si_2$; Hexaet) and hexamethoxydisilane ($C_6H_{18}O_6Si_2$; Hexamet) were purchased from ABCR GmbH & Co. KG (Germany) and used as received. All other chemicals were of analytical reagent grade. One set of bulk samples was prepared for each of the two above-mentioned precursors.

Two sets of samples were prepared, one for each of the silane precursors mentioned above. Set 1 was made as follows. The *sol* solution was prepared by mixing Hexaet with ethanol (EtOH) in a 2:1 ratio (v:v). The resulting solution was subsequently diluted two-fold in acidic water pH 5 (DI water pH was adjusted to five with diluted HCl) and then was vigorously stirred at room temperature in a sealed disposable beaker for 2 h. During this step, the material started to condense. After that, small holes were opened in the lid of the beaker and the polymer material was left to further condense and age for at least 2 days at room temperature, until a solid was obtained. Finally, the sol–gel material was dried in a furnace at 80 °C for 48 h. Set 2 samples were prepared using the same protocol but exchanging the Hexaet silane precursor by the Hexamet one. For both sets, the resulting as-synthesized materials were then annealed in a N_2 atmosphere for 1 h at temperatures in the range 350–1,300 °C. The raising and decreasing temperature rates were 5 °C/min from and up to room temperature, respectively. This sol–gel synthesis process can be considered as environmentally friendly since both silane precursors are innocuous, they can be manipulated under room laboratory conditions and the prepolymerization solution was prepared just in an ethanol–water solution.

2.2 Photoluminescence studies

PL spectra in the range of 350–1,000 nm were obtained by means of an Ocean Optics QE65000 spectrometer with an integration time of 1 s, unless stated otherwise. They were corrected with the spectral response of the setup. Continuous wave excitation was accomplished by using the 325 nm line of a 30 mW He–Cd laser. A 350 nm long pass filter was utilized to eliminate laser radiation from the emergent beam, which was collected by a lens system and directed to a microscope objective coupled to a 1 mm silica core optical fiber.

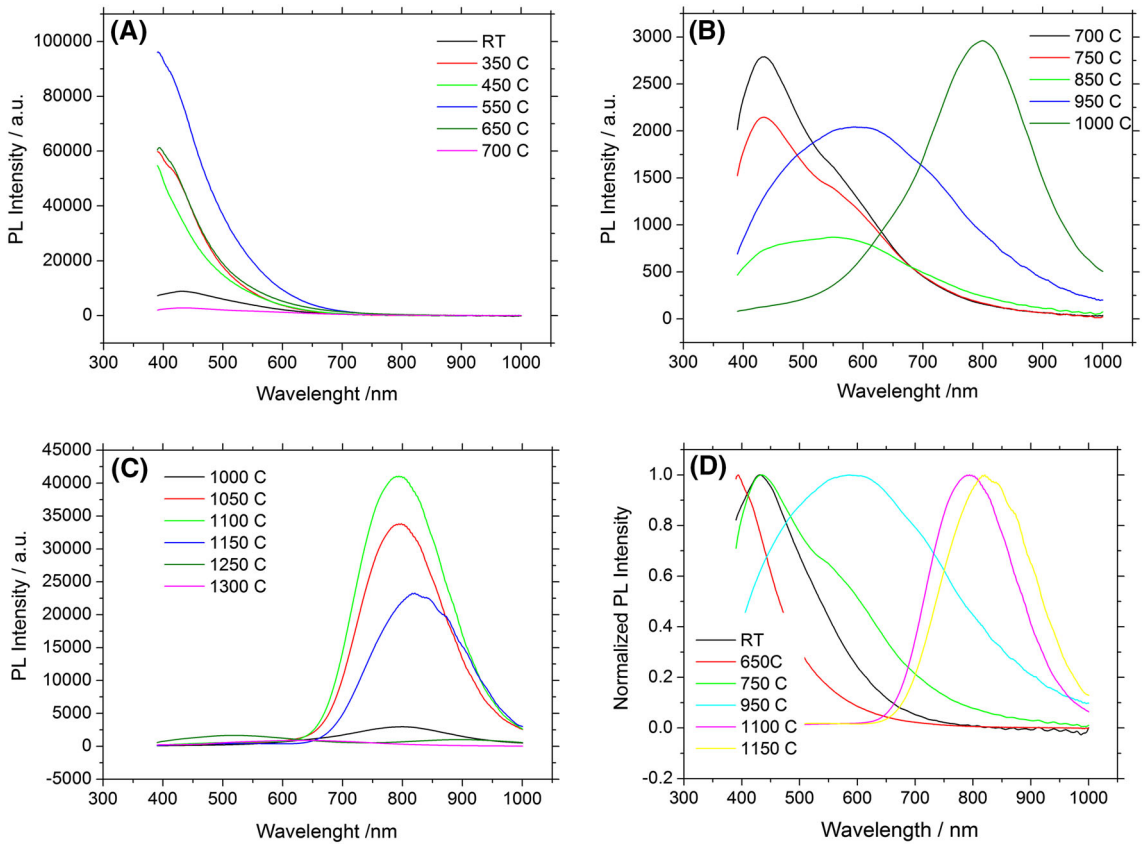

Fig. 1 **a–c** Photoluminescence spectra of Hexaet-derived materials annealed at different temperatures. Spectra at Ts of 700 and 1,000 °C are repeated in **a**, **b** and **b**, **c**, respectively, for comparison purposes. These T were chosen on the basis of the significant changes taking place in the luminescent behavior of the material (**d**) Normalized response

2.3 Structural characterization

ATR-FTIR spectra were obtained with a Bruker spectrophotometer, model TENSOR27 (Bruker Optics GmbH, Germany), including an attenuated total reflectance module (ATR), in the range 500–4,500 cm^{-1} with a resolution of 2 cm^{-1}. TEM micrographs were obtained in a JEM 2011 microscope (Jeol Ltd., Japan) at 200 kV acceleration voltage and 0.18 nm resolution. XPS analysis was carried out in a K-Alpha—Thermo Scientific spectrometer (Thermo Fisher Scientific Inc., USA) using a monochromatized Al Kα source (1,486.6 eV). Survey spectra and spectra of Si and O peak regions were recorded at pass energies of 200 and 50 eV, respectively. Irradiation was carried out perpendicular to the sample surface, the sample spot diameter being 50 µm. Samples were previously etched with a beam of Ar^+ ions in order to neglect possible contributions from adsorbed gaseous species on the material surface. The percentages of the different elements in the samples were calculated using the atomic sensitivity factors provided by the XPS equipment. Elemental chemical analysis was carried out using a CHNS Thermo Scientific Flash 2000 analyzer (Thermo Fisher Scientific Inc., USA). Some 0.7–2.7 mg of each material were burned in an oxygen atmosphere at 1,200 °C and the resulting combustion products analyzed by gas chromatography.

3 Results

Figure 1 depicts the room temperature PL behavior of Hexaet-derived materials (set 1), as synthesized and annealed at temperatures in the range 350–1,300 °C. Spectra were split into three graphs depending on the T annealing range, for clarity of presentation. The spectral response in Fig. 1a for those materials annealed between RT and 700 °C shows a band peaking at ca. 430 nm. Upon increasing the T stepwise from 700 to 1,000 °C, this band was firstly divided into two overlapped signals and in turn shifted towards longer wavelengths, with all bands peaking below 600 nm (Fig. 1b). It is worth noting how the PL intensity abruptly decreased for the material at 700 °C and was kept very low for all those ones synthesized in the 700–1,000 °C range. Six materials were prepared and annealed in the range from 1,000 to 1,300 °C. Here a single band peaking at ca. 800 nm was recorded. It can be seen in

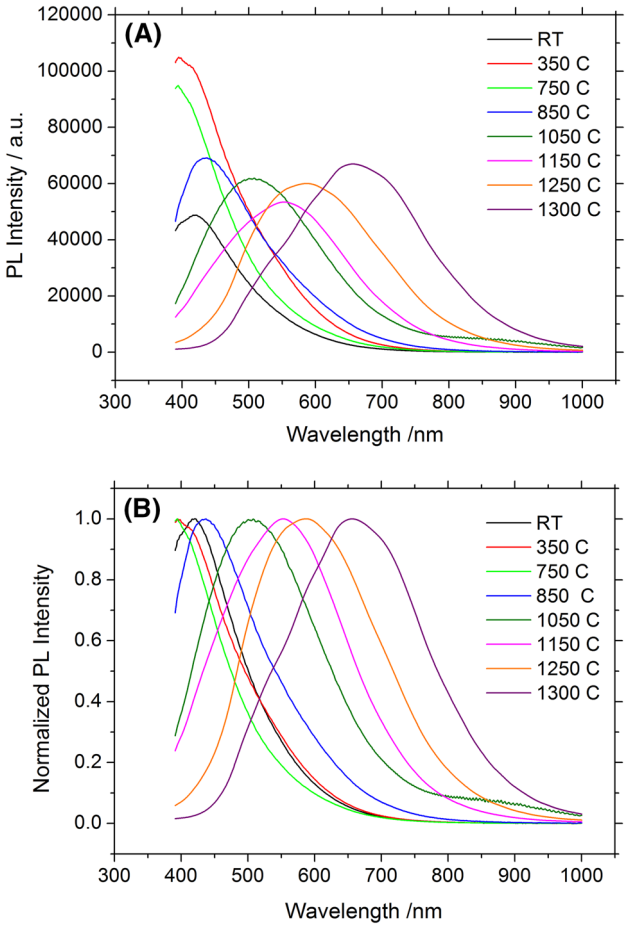

Fig. 2 **a** Photoluminescence spectra of Hexamet-derived materials. **b** Normalized response

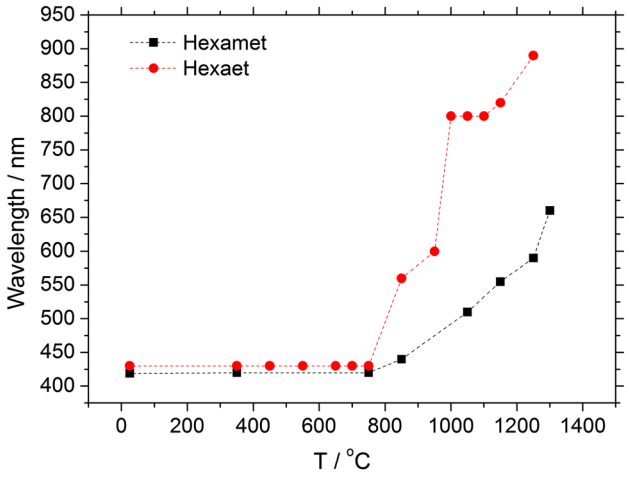

Fig. 3 Dependence of the PL band with the material annealing T

Fig. 1c that the corresponding PL intensity sharply increased for those samples annealed at T up 1,150 °C and then it decreased and was very low for those ones treated at higher Ts (1,250 and 1,300 °C). Figure 1d shows the normalized signals of those representative materials in the whole T range tested, where the shift of the PL band peak can be clearly compared.

Figure 2 shows the PL spectra of Hexamet-derived materials (set 2) prepared and recorded under the same experimental conditions as those for Hexaet-derived samples. The intense band peaking at wavelengths below 450 nm was also observed with these materials annealed at T below 850 °C (Fig. 2a). At higher Ts, the band shifted to longer wavelengths, showing peaks between 500 and 650 nm. Figure 2b also shows the normalized signals to better compare the changes in the PL band wavelength of all the tested Hexamet-derived materials.

Table 1 gathers spectra relevant information such as the wavelength for the different PL bands shown in Figs. 1 and 2, as well as those structures that might be related for them. In order to better visualize the shift of the PL peak wavelength with the annealing T, Fig. 3 is also included. Similarities as well as important differences are observed for both sets of materials, depending on the thermal process parameters, as will be discussed in the next section.

Table 1 Photoluminescence bands identified in the spectra of Figs. 1 and 2, and the types of defects that can be associated with according to literature

Wavelength/nm (eV)	Sample (T range/°C)	Association	References
430 (2.90)	Hexaet (RT-850)	Oxygen deficient centers	[23, 24]
	Hexamet (RT-850)		
507 (2.44)	Hexamet (1,050)	E' centers or H defects	[25, 26]
550 (2.25)	Hexaet (700–850)		
	Hexamet (1,150)		
590 (2.10)	Hexaet (950)	H defects (Si–OH, Si–H)	[25]
	Hexamet (1,250)		
650 (1.90)	Hexamet (1,350)	Non-bridging oxygen hole centers (NBOHC)	[27, 28]
800 (1.55)	Hexaet (1,000–1,100)	Si nanoclusters	[19, 29, 30]
820 (1.50)	Hexaet (1,150)		
857 (1.44)	Hexaet (1,150 for 3 h)		

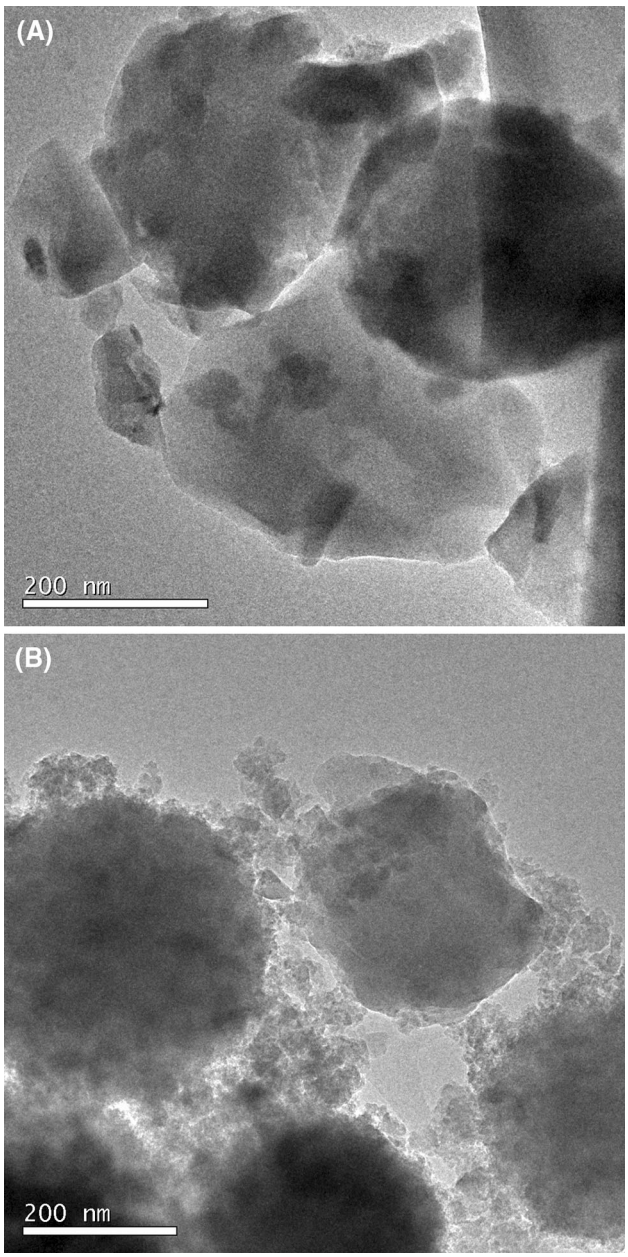

Fig. 4 Low magnification TEM images of as-synthesized **a** Hexaet- and, **b** Hexamet-derived materials

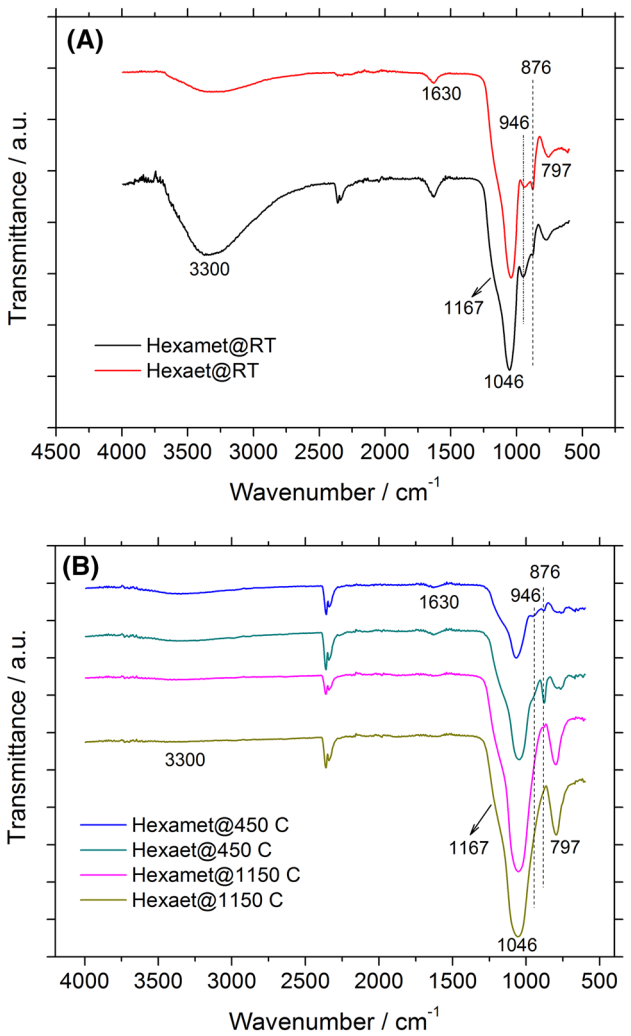

Fig. 5 ATR-FTIR spectra of the, **a** as-synthesized materials and, **b** those annealed at 450 and 1,100 °C

The different behavior shown in the materials prepared using each precursor, especially those annealed at T above 1,000 °C might be related to the different structures of the initial polymeric matrices. Figure 4 shows TEM images of as-synthesized materials. The Hexaet-derived material shows a more uniform structure while the Hexamet-derived one appeared to be formed by aggregation of sub-micron sized particle units.

ATR-FTIR spectra of the as-synthesized polymers also accounts for these similarities and differences between the two materials (Fig. 5). Two more intense bands at 1,630 and 3,300 cm^{-1} were recorded with the as-synthesized Hexamet- material, these being ascribed to the water and silanol (Si-OH) group content of the material, respectively. A close-up look to the bands that appear in the 1,400–600 cm^{-1} region of the spectra of the as-synthesized materials and those annealed at two representative temperatures, that is 450 and 1,150 °C, reveal four characteristic bands at 797, 876, 946, 1,046 and 1,167 cm^{-1}.

Table 2 summarizes this information together with the assignments for each band that have been previously reported in the literature. Important differences due to the intensity and presence or absence of some of these bands also account for the different structural and luminescent behavior of the tested materials. Among them, that one at 876 cm^{-1} may be related to the presence of defects in the SiO_2 structure.

XPS studies were also carried out to give more insight about the structural differences of the synthesized materials. Spectra corresponding to Hexamet- and Hexaet-

Table 2 FT-IR bands identified in the spectra of the sol–gel materials and their corresponding assignments

Wavenumber/ cm^{-1}	Assignment	Reference
797	v_s(Si–O–Si)	[31, 32]
876	Si–OH	[31, 32]
	Si_2O_3 (sub-oxidized Si species)	[33]
	H–Si–O hybrid vibration (830–875 cm^{-1})	[31]
	Si–H (usually between 700 and 1,010 cm^{-1})	[34]
946	v(Si–OH)	[31, 32]
1,046	v_{as}(Si–O–Si)	[31, 32]
1,167	v_{as}(Si–O–Si)	[31, 32]
1,630	δ(H–O–H)	[34]
3,300	v(Si–OH)	[32]

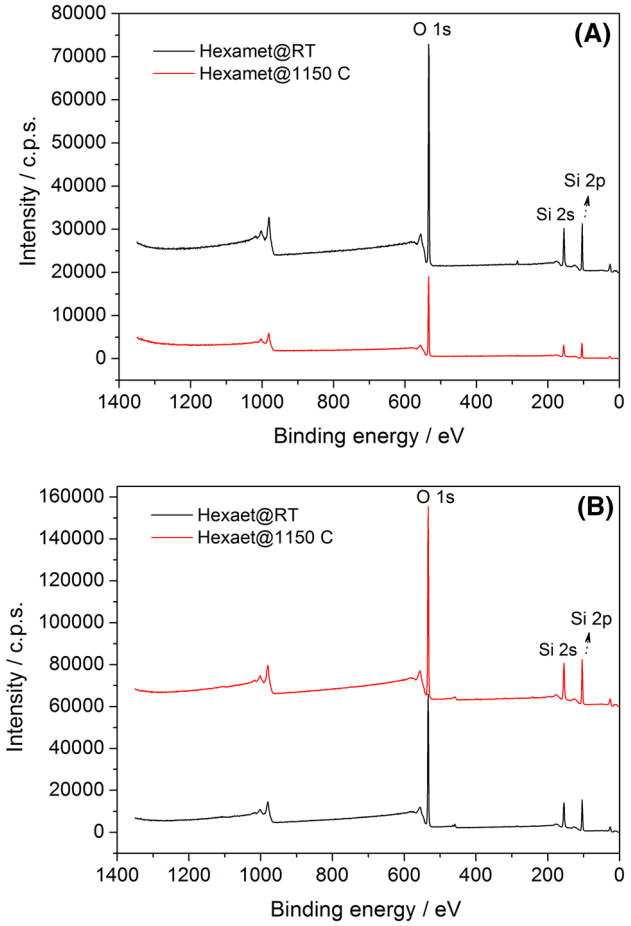

Fig. 6 XPS survey spectra of **a** Hexamet-derived and **b** Hexaet-derived materials as synthesized and annealed at 1,150 °C

materials, as-synthesized and annealed at 1,150 °C are shown in Fig. 6. Three signals corresponding to Si_{2p}, Si_{2s} and O_{1s} were clearly visible in all the spectra. These were centered at around 104 eV, 154 eV and 533 eV,

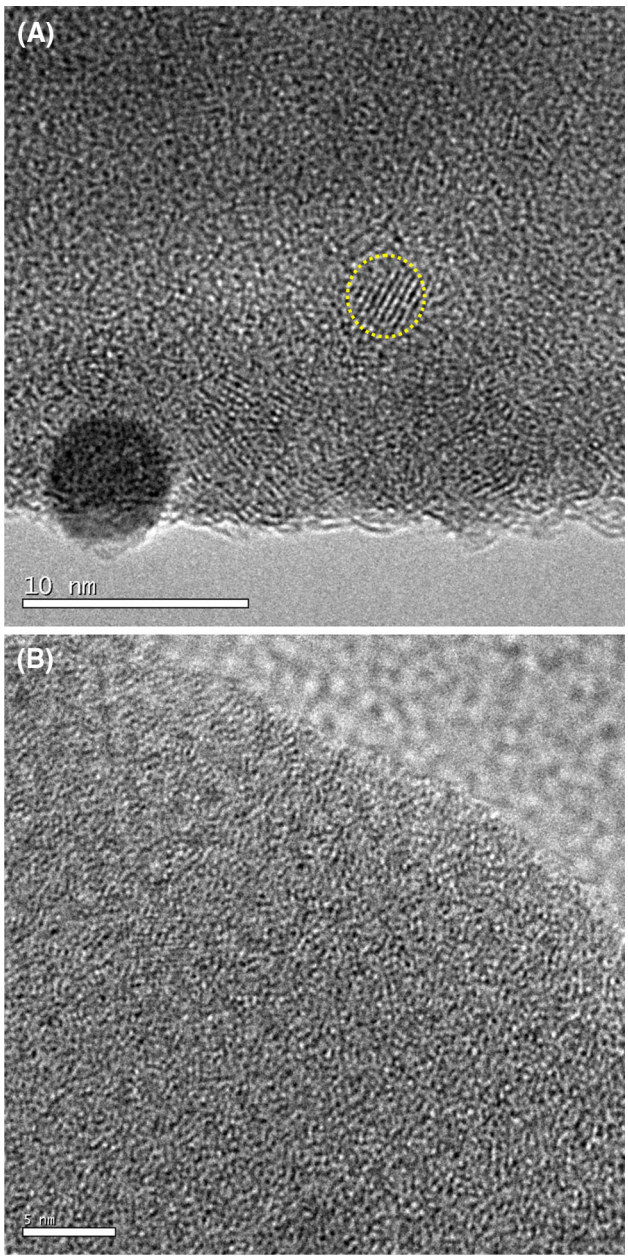

Fig. 7 HRTEM images of the Hexaet-derived material (**a**) and Hexaet-derived material (**b**) annealed at 1,150 °C

respectively, which appear to correspond to a SiO_2 gel basic structure (data extracted from LASURFACE.com database), as is the case considering the sol–gel synthesis process carried out in this work. The XPS analysis of the as-synthesized Hexaet-derived material showed a roughly 7.3 % Si excess in a substoichiometric SiO_2 structure whereas this excess decreased to around 3.7 % in the Hexamet-derived material counterpart. The Si excess values were kept nearly constant in both the Hexaet-derived (ca. 7.0 %) and the Hexamet-derived (ca. 3.0 %) materials annealed at 1,150 °C.

Scheme 1 Sol–gel acidic hydrolysis

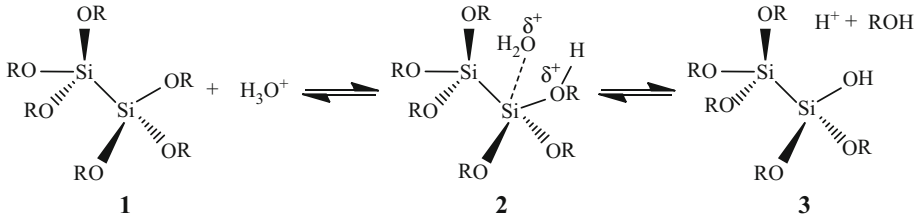

Figure 7 shows a high resolution TEM (HRTEM) micrograph of a Hexaet-based sample annealed at 1,150 °C, in which some nanocrystals are observed. In particular, a nanocrystal of about 3 nm diameter with an interplanar distance of about 0.34 nm (measured with the HRTEM analysis software), attributed to crystalline silicon (111) planes, is labelled. As mentioned above, the presence of Si_nc for samples of this set annealed at 1,050–1,150 °C was previously demonstrated by Raman and TR-PL Spectroscopic techniques, as explained in Ref. [22]. The spectral behavior for Hexamet-based samples (set 2) is completely different. The presence of Si_nc was observed neither by HRTEM nor by Raman and TR-PL Spectroscopies at any annealing temperature.

4 Discussion

4.1 Mechanisms behind the material syntheses

The sol–gel chemical process that rules the formation of the as-synthesized materials presented in this work could explain the similarities in their recorded PL luminescent behavior but also the marked dissimilarities found upon these materials were submitted to an annealing process in a wide T range. Hexaethoxydisilane and hexamethoxydisilane share a structurally equivalent generic basic unit (Scheme 1, **1**). The processes of hydrolysis and condensation reactions taking place during the polymer formation with both precursors were analyzed in detail.

Both molecules are silane monomers of the type $(OR)_3Si–Si(OR)_3$, where –OR is a hydrolysable ethoxy or methoxy group, respectively. It is known that the kinetics of the hydrolysis and condensation reactions strongly depends on the solution pH [35]. At the acidic pH used in this work, the alkoxy (ethoxy or methoxy; –OR) group could be protonated, so that a water molecule could react with a silane molecule and carry out a nucleophilic substitution with one of these groups, thus liberating an alcohol molecule (ethanol or methanol; ROH) and generating a silanol group (Si–OH) (Scheme 1, **3**). These reactions are relatively slow in acidic medium, considering the intermediate species and their relative stability [35]. Nevertheless, the kinetics of these reactions is also strongly dependent on the –OR group.

Considering just the solution pH and taking into account that –OR groups are more electron donating than hydroxyl groups (–OH), the more –OR groups replaced by –OH groups, the less stabilized the transition state (Scheme 1, **2**), and so the hydrolysis reaction rate decreases in the order of $(OR)_2(OH)Si–Si(OH)(OR)_2 > (OR)(OH)_2Si–Si(OH)_2(OR) > (OH)_3Si–Si(OH)_3$). This makes the first hydrolysis reaction to be the fastest and the generated –OH group rapidly condense with another –OH group to give rise to a siloxane ($\equiv$Si–O–Si$\equiv$) species (Scheme 2, **4**), in turn liberating a water molecule. This polymerization process gives rise to open linear-like polymer structures, which eventually cross-linked upon hydrolysis of the other –OR groups, thereby resulting in dense, compact, homogeneous and transparent silicon oxide-based polymer structures.

However, as mentioned above, due to steric effects being different for methoxy- and ethoxy-groups, methoxy groups are more prone to be protonated, this making the hydrolysis reaction rate to be faster than that involving the ethoxy groups. Therefore, it is more likely that when working with hexamethoxydisilane other intermediate species resulting from several hydrolysis reactions underwent by the same molecule, such as $(OR)(OH)_2Si–Si(OH)_2(OR)$ or $(OH)_3Si–Si(OH)_3$ are being produced before the condensation reactions take place. This effect gives rise to the initial formation of polymer condensation points (highly cross-linked polymeric particles) from which the polymer grows and cross-links to eventually form an opened and highly porous opaque silicon oxide-based polymer structure.

Such differences could be clearly visualized in the as-synthesized Hexamet- and Hexaet-derived materials under the naked eye. The former was a white opaque and to a certain degree dust-like material, whereas the latter was a hard, dense and translucent solid. Also, the low-magnification TEM images in Fig. 3 show particle-like and more uniform structures in each material, respectively. These differences still persisted following the annealing processes. Nevertheless, a mechanically stable ceramic material was produced in both cases.

Scheme 2 Sol–gel condensation reaction

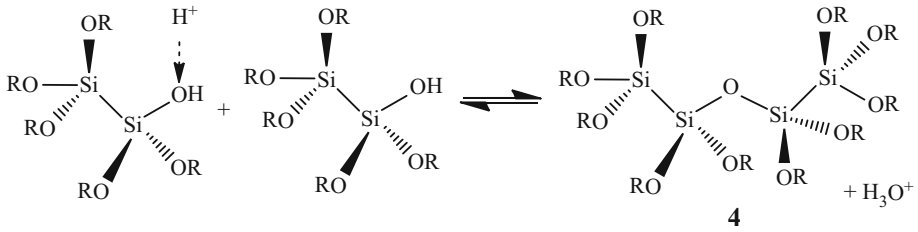

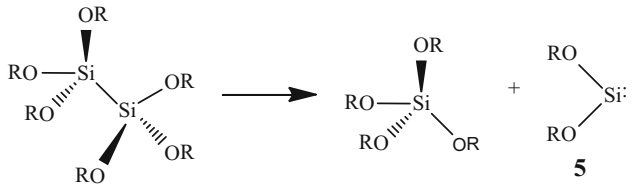

Scheme 3 Silylene formation from a hexalkoxydisilane

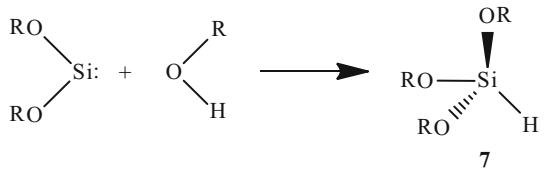

Scheme 5 Silylene insertion in an O–H bond

It has been previously reported that, upon a thermal treatment carried out at T around 200 °C or below, both hexaethoxydisilane and hexamethoxydisilane could form reactive species called silylenes (Scheme 3, **5**) [36]. These molecules are unstable and highly reactive [37]. On one hand, it has been demonstrated that they rapidly react by insertion with Si–O bonds and produce trisilane structures (Scheme 4, **6**) [38]. On the other hand, they could insert into O–H bonds of alcohol molecules present in the sample and generate Si–H bonds in the polymeric network (Scheme 5, **7**) [36, 39]. Both chemical reactions would give rise to completely different defects in the resulting SiO_2 polymeric structure that would account for the PL luminescence performance, as explained below.

4.2 Structural and luminescent analysis of materials as synthesized and annealed in the range of 350–750 °C

The structural characterization carried out with both materials support the above synthetic processes. The FT-IR absorption bands of the as-synthesized materials with maxima around 3,300 and 1,630 cm^{-1} are assigned to the –OH bond stretching and H_2O bending, respectively (Table 2). It can be seen in Fig. 5a that the Hexamet-derived material contains more water and a significantly higher amount of –OH groups that may be ascribed to free silanol (≡Si–OH) groups in the polymer matrix. This would be in agreement with the higher degree of hydrolysis of the methoxy groups, mentioned above. In this context, another side effect could be taking place. –OH groups bound to a Si atom are more electron withdrawing than the corresponding –OR counterparts, which makes the Si–Si bond to be more unstable. Taking into consideration the bond dissociation energies of both Si–Si and Si–O bonds [40], it could be assumed that Si–Si bonds can be more easily hydrolyzed as the number of –OH groups bound to each Si atom increases. Thus, this is more likely to happen when synthesizing Hexamet-derived materials. Indeed, this assumption is in agreement with results obtained from the XPS analysis shown in Fig. 6 that indicate a higher Si excess in a substoichiometric SiO_2 structure for the as-synthesized Hexaet-derived material than for the Hexamet-derived material counterpart.

Both ≡Si–Si≡ and Si–OH species likely present in the as-synthesized materials, as described above, can be considered as oxygen deficient centers of a SiO_2 network [41]. It has been reported that these defects may be responsible for the blue PL recorded at around 2.90–3.20 eV (430–390 nm) [23, 24]. The PL spectral behavior observed

Scheme 4 Silylene insertion in a Si–O bond

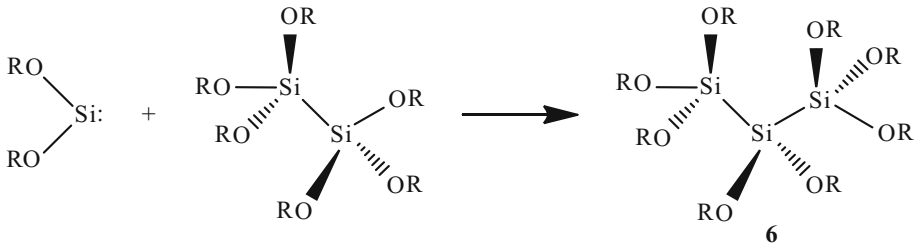

for Hexaet- and Hexamet-derived materials, as-synthesized and annealed in the temperature range from 350 to 750 °C (please, compare Fig. 1a, b and 2a and see values in Table 1) show bands in this region. However, the PL intensity differs in both materials and also seems to depend on the material annealing T. Hexaet-derived samples show PL spectra whose intensity is significantly low for those as-synthesized, annealed at 700 and 750 °C comparing with that recorded with those ones annealed in the 350–650 °C range. Considering the hydrolysis and condensation reactions taking place with this material and the fact that the as-synthesized sample may contain a certain amount of non-hydrolyzed ethoxy groups, as pointed out above, the annealing processes in the 350–650 °C range might promote the generation of Si–OH groups and in turn an increase of the PL intensity. Upon raising the annealing T, these groups may further condense to give siloxane (≡Si–O–Si≡) bonds, which would result in decrease of the material PL intensity. Hexamet-derived materials, which contain a higher amount of Si–OH groups in the as-synthesized sample, show a higher PL intensity than that recorded with the as-synthesized Hexaet-derived counterpart (Fig. 2a). When the annealing T is raised up to 750 °C, more Si–OH groups may be generated in the sol–gel matrix and their subsequent condensation induced the initial increase and subsequent decrease of the recorded PL intensity, respectively.

However, other simultaneous reactions could be taking place in this T range (350–750 °C) considering that the absorbance values of those ATR-FTIR peaks at 3,300 and 1,630 cm^{-1}, assigned to the –OH and H_2O species, significantly decreased for both materials when annealed at 450 °C (Fig. 5b). It has been reported that oxygen deficient centers of different nature could be created in the annealing T range used in the preparation of these samples (Table 1 and references therein), which might contribute to the changes of the photoluminescence behavior shown in Figs. 1 and 2.

ATR-FTIR spectra of Hexamet- and Hexaet- derived materials synthesized at different Ts, show four bands in the region between 600 and 1,400 cm^{-1} (Fig. 5), which can be assigned to the bending and stretching of Si–OH and Si–O-Si bonds, in accordance with previously reported works about the characterization of SiO_2-based structures (Table 2 and references therein). Moreover, a fifth band at around 876 cm^{-1} was also identified. A literature search about the assignments of this band evidenced that this band could be related to the vibration of Si–O bonds in free silanol groups in a silicon oxide structure but also to Si–Si bonds in sub-oxidized silicon structures (≡Si–Si≡) or Si–H bonds (Table 2 and references therein). The presence of these ≡Si–Si≡ and Si–H chemical moieties in the material structures would be in agreement with the formation of silylene intermediates and the trapping of these highly reactive species by insertion into Si–O and O–H bonds, respectively, as explained in the previous section. In this context, the band is clearly visible in the spectra of the as-synthesized Hexaet-derived and Hexamet-derived materials. By contrast, a more accentuated band appeared in the spectrum of the Hexaet-derived material annealed at 450 °C while it fades in the spectrum of the Hexamet-derived one annealed at the same T. Whether this band is assigned to sub-oxidized silicon species would suggest a higher density of Si–Si bonds in the as-synthesized Hexaet-derived material. If Si–H bonds are responsible for this band, this is also more likely to take place in the Hexaet-derived material than in the Hexamet-based one.

4.3 Structural and luminescent analysis of materials annealed in the range of 750–1,300 °C

The PL behavior of the Hexaet-derived materials (Fig. 1b and 1c) and Hexamet-derived materials (Fig. 2b) annealed in this T range significantly changed with respect to that one shown in the materials synthesized at lower T. These differences could also be explained on the basis of structural changes taking place during the annealing process and that have been described above. Green-yellow PL bands peaking at 507, 550 and 590 nm, that appeared in the spectra of these materials have been previously ascribed to E' centers and H defects present in the material structure (Table 1 and references therein). Hexamet-derived samples annealed at Ts between 1,050 and 1,250 °C clearly showed such behavior. Indeed, ATR-FTIR spectrum of the Hexamet-derived sample annealed at 1,100 °C shows a small band at 876 cm^{-1}, which pointed out that Si–H bonds are still present in the sample. This was confirmed by elemental chemical analysis that showed the unambiguous presence of H, which would then be an indication of the presence of such kind of defects in the structure of the Hexamet-derived materials. Similarly, Hexaet-derived materials annealed in the T range between 700 and 950 °C also show these bands.

However, the PL spectra of Hexaet-derived materials annealed at 1,000 and above and Hexamet-derived ones at 1,250 °C and above are radically different (Figs. 1c, 2a). The PL maximum of Hexaet-derived samples drastically red shifts to about 800 nm when the temperature increased from 950 to 1,000 °C (Table 1) and the PL intensity drastically raises from 1,050 °C on, with a maximum value at 1,100 °C. The shape-line and spectral position of these spectra clearly suggest the evolution toward a radiative mechanism by quantum confinement in Si nanocrystals (Si_nc) embedded in a SiO_2 matrix (Table 1 and references therein). The disappearance of the ATR-FTIR band at 876 cm^{-1} for the Hexaet-derived sample annealed at

1,100 °C evidenced the consumption of Si–H bonds at such high T and the diffusion of Si within the material matrix to generate Si_nc, as previously reported [42]. This process was confirmed by elemental chemical analysis showing that no H was present in the sample chemical structure. Also, the HRTEM micrograph in Fig. 7a show the presence of Si_nc for a sample of the Hexaet-derived material annealed at 1,150 °C. As already mentioned above, the formation of these nanostructures was previously demonstrated by Raman and TR-PL spectroscopies [22].

The annealing temperature has a decisive influence on the crystal growth process and consequently on its eventual size. Indeed, it is suggested that Si_nc are auto-assembled from individual atoms due to processes of Si diffusion, nucleation and crystallization. These processes are thermally stimulated. An evidence of this phenomenon can also be shown in the decrease of the PL intensity when the material was annealed at 1,150 °C and the weak signals recorded with those ones annealed at 1,250 and 1,300 °C. This suggests the increase of the Si_nc particle size with T, which in turn induced the red shift of the PL band shown in the spectra in the 1,150–1,300 °C T range as well as the decrease of the quantum confinement effect that was eventually lost when the T was raised to 1,300 °C.

Hexamet-derived materials did not contain any Si_nc as evidenced by HRTEM (Fig. 7b) and by Raman Spectroscopy [22]. Furthermore, PL spectra peaked below 700 nm even for samples annealed at T as high as 1,350 °C (PL band at 650 nm, Table 1), which can be considered as an indication of absence of a quantum confinement radiative mechanism. Consequently, the presence of other mechanisms possibly associated to defects of the silicon oxide matrix such as non-bridging oxygen hole centers (NBOHC), as previously reported (Table 1 and references therein), may be considered.

XPS analysis of samples annealed at 1,150 °C were also in agreement with these structural differences that would give rise to such different photoluminescence behavior (Fig. 6). The values of Si excess of both materials were of the same order of magnitude to those shown by the as-synthesized materials, which points out that the different kinetics of hydrolysis and condensation during the corresponding sol–gel syntheses were responsible for such drastic change in their luminescent performance.

As a useful overview of the material PL shift taking place with the annealing T, the normalized responses of Hexaet- and Hexamet-derived materials are shown in Figs. 1d and 2b. Also, the dependence of the PL peak wavelength with T is depicted in Fig. 3. It is clearly seen how the spectra of both materials shifted to higher wavelengths as the T was increased. However, in the Hexaet-derived material, a radical change took place when this T was above 1,000 °C, which, as described above, was directly related to the formation of Si nanocrystals. Deconvolution of the PL spectrum recorded at 1,150 °C showed two peaks at 780 nm and 850 nm, with relative areas of 0.26 and 0.74, respectively. These values unambiguously point out to the luminescence being mainly related to quantum confinement in the nanocrystals. By contrast, in the Hexamet-derived material, PL maxima are always below 800 nm. Deconvolution of the corresponding PL spectrum at 1,150 °C also showed to peaks at 548 nm and 754 nm, with relative areas of 0.95 and 0.05, respectively. From this data, the luminescence could solely be associated to defects present in the material structure.

5 Conclusion

Two sets of luminescent silica-based sol–gel materials were synthesized using two different silane monomers both bearing a Si–Si bond and compared in terms of their luminescent performance. The mechanisms that govern the different luminescent behavior appear to be related to significant structural differences between the two sets of materials, as supported by ATR-FTIR, XPS, HRTEM and elemental chemical analyses. The different kinetics of the reactions taking place during the corresponding sol–gel syntheses may be responsible for such differences. These reactions could be modulated so that materials with tailor-made luminescent performance could be easily synthesized. The simple and cost-effective sol–gel process applied in this work as well as the excellent luminescent properties of the resulting materials make the presented approach to be of practical use for the inexpensive fabrication of light sources, provided that the corresponding efficiency studies are achieved. Additionally, this sol–gel process is compatible with microfabrication techniques and as such could be implemented for the integration of these components into photonic integrated circuits.

Acknowledgments Financial support from MINECO-DGI, Project Ref. TEC2010-17274 and CSIC, Project Ref. PIE 200950I197, is acknowledged.

References

1. Canham LT (1990) Silicon quantum wire array fabrication by electrochemical and chemical dissolution of wafers. Appl Phys Lett 57:1046–1048
2. Dinh LN, Chase LL, Balooch M, Siekhaus WJ, Wooten F (1996) Optical properties of passivated Si nanocrystals and SiOx nanostructures. Phys Rev B 54:5029–5037
3. Torchynska T, Becerril Espinoza FG, Goldstein Y, Savir E, Jedrzejewski J, Khomenkova L, Korsunska N, Yukhimchuk V (2003) Nature of visible luminescence of co-sputtered Si–SiOx systems. Phys B 340:1119–1123

4. Chen MJ, Yen JL, Li JY, Chang JF, Tsai SC, Tsai CS (2004) Stimulated emission in a nanostructured silicon pn junction diode using current injection. Appl Phys Lett 84:2163–2165
5. Dal Negro L, Yi JH, Kimerling LC, Hamel S, Williamson A, Galli G (2006) Light emission efficiency and dynamics in silicon-rich silicon nitride films. Appl Phys Lett 88:183103
6. Torchynska TV, Vivas Hernandez A, Goldstein Y, Jedrzejewskii J, Sandoval SJ (2006) Photoluminescence of Si or Ge nanocrystallites embedded in silicon oxide. J Non-Crystal Solids 352:1152–1155
7. Hessel CM, Henderson EJ, Kelly JA, Cavell RG, Sham T-S, Veinot JGC (2008) Origin of luminescence from silicon nanocrystals: a near edge X-ray absorption fine structure (NEXAFS) and X-ray excited optical luminescence (XEOL) study of oxide-embedded and free-standing systems. J Phys Chem C 112:1 4247–14254
8. Miska P, Dossot M, Nguyen TD, Grün M, Rinnert H, Vergnat M, Humbert B (2010) Embedded silicon nanocrystals studied by photoluminescence and Raman spectroscopies: exciton and phonon confinement effects. J Phys Chem C 114:17344–17349
9. Prokes SM (1993) Light emission in thermally oxidized porous silicon—evidence for oxide-related luminescence. Appl Phys Lett 62:3244–3246
10. Zyubin AS, Glinka YD, Mebel AM, Lin SH, Hwang LP, Chen YT (2002) Red and near-infrared photoluminescence from silica-based nanoscale materials: experimental investigation and quantum-chemical modeling. J Chem Phys 116:281–294
11. Hill NA, Whaley KB (1995) Size dependence of excitons in silicon nanocrystals. Phys Rev Lett 75:1130–1133
12. Linnros J, Priolo F, Canham L (1998) Light emission from silicon: progress towards Si-based optoelectronics. In: Proceedings of E-MRS 1998, Elsevier, Amsterdam, 1999
13. Pavesi L, Dal Negro L, Mazzoleni C, Franzo G, Priolo F (2000) Optical gain in silicon nanocrystals. Nature 408:440–444
14. Wolkin MV, Jorne J, Fauchet PM, Allan G, Delerue C (1999) Electronic states and luminescence in porous silicon quantum dots: the role of oxygen. Phys Rev Lett 82:197–200
15. Prokes SM, Glembocki OJ, Bermudez VM, Kaplan R, Friedersdorf LE, Searson PC (1992) Sihx excitation—an alternate mechanism for porous Si photoluminescence. Phys Rev B 45:13788–13791
16. Brandt MS, Fuchs HD, Stutzmann M, Weber J, Cardona M (1992) The origin of visible luminescence from porous silicon—a new interpretation. Solid State Commun 81:307–312
17. Schottner G (2001) Hybrid sol–gel-derived polymers: applications of multifunctional materials. Chem Mater 13:3422–3435
18. Soraru GD, Modena S, Bettotti P, Das G, Mariotto G, Pavesi L (2003) Si nanocrystals obtained through polymer pyrolysis. Appl Phys Lett 83:749–751
19. Das G, Ferraioli L, Bettotti P, De Angelis F, Mariotto G, Pavesi L, Di Fabrizio E, Soraru GD (2008) Si-nanocrystals/SiO2 thin films obtained by pyrolysis of sol–gel precursors. Thin Solid Films 516:6804–6807
20. Dian J, Valenta J, Luterova K, Pelant I, Nikl M, Muller D, Grob JJ, Rehspringer JL, Hónerlage B (2000) Optical properties of Si+-ion implanted sol–gel derived SiO_2 films. Mater Sci Eng B 69:564–569
21. Dima A, Della Corte FG, Williams CJ, Watkins KG, Deardena G, O'Hare N, Casalino M, Rendina I, Dima M (2008) Silicon nanoparticles in SiO2 sol–gel film for nano-crystal memory device applications. J Microelectron 39:768–770
22. Rodríguez JA, Fernández-Sánchez C, Domínguez C, Hernández S, Berencén Y (2012) Bulk silica-based luminescent materials by sol–gel processing of non-conventional precursors. Appl Phys Lett 101:171908
23. Lin G-R, Lin C-J, Yu K-C (2004) Time-resolved photoluminescence and capacitance-voltage analysis of the neutral vacancy defect in silicon implanted SiO_2 on silicon substrate. Appl Phys Lett 96:3025–3027
24. Skuja L (1998) Optically active oxygen-deficiency-related centers in amorphous silicon dioxide. J Non-Cryst Solids 239:16–48
25. Hinić I, Stanišić G, Popović Z (2003) Influence of the synthesis conditions on the photoluminescence of silica gels. J Serb Chem Soc 68:953–959
26. Yu Z, Aceves M, Carrillo J, Flores F, Falcony C, Domínguez C, Llobera A, Morales-Acevedo A (2004) Photoluminescence in off-stoichiometric silicon oxide compounds. Superficies y Vacio 17: 1–6
27. Suzuki T, Skuja L, Kajihara K, Hirano M, Kamiya T, Hosono H (2003) Electronic structure of oxygen dangling bond in glassy SiO(2): the role of hyperconjugation. Phys Rev Lett 90:186404
28. Vaccaro L, Morana A, Radzig V, Cannas M (2011) Bright visible luminescence in silica nanoparticles. J Phys Chem C 115: 19476–19481
29. Lau HW, Tan OK, Liu Y, Ng CY, Chen TP, Pita K, Lu D (2005) Defect-induced photoluminescence from tetraethylorthosilicate thin films containing mechanically milled silicon nanocrystals. J Appl Phys 97:104307
30. Yi LX, Heitmann J, Scholz R, Zacharias M (2002) Si rings, Si clusters, and Si nanocrystals-different states of ultrathin SiOx layers. Appl Phys Lett 81:4248–4250
31. Bornhauser P, Calzaferri G (1996) Ring-opening vibrations of spherosiloxanes. J Phys Chem 100:2035–2044
32. Dohnalová K, Pelant I, Kůsová K, Gilliot P, Gallart M, Crégut O, Rehspringer J-L, Hönerlage B, Ostatnický T, Bakardjeva S (2008) Closely packed luminescent silicon nanocrystals in a distributed-feedback laser cavity. New J Phys 10:063014
33. Luna-López JA, Carrillo-López J, Aceves-Mijares M, Morales-Sánchez A, Falcony C (2009) FTIR and photoluminescence of annealed silicon rich oxide films. Superficies y Vacío 22:11–14
34. Pretsch E, Buhlmann P, Badertscher M (2009) Structure determination of organic compounds: tables of spectral data, 4th edn. Springer, Berlin
35. Wright JD, Sommerdijk NAJM (2000) Advanced chemistry text series. In: Phillips D, O'Brien P, Roberts S (eds) Sol–gel materials chemistry and applications, vol 4. CRC Press, Florida
36. Atwell WH, Weyenberg DR (1968) Silylene chemistry I. thermolysis of methoxypolysilanes. J Am Chem Soc 90:3438
37. Gillette GR, Noren GH, West R (1989) Lewis base adducts to diorganosilylenes. Organomet 8:487–491
38. Atwell WH, Mahone LG, Hayes SF, Uhlmann JG (1969) Silylene chemistry 2. A kinetic study of thermolysis of sym-dimethoxytetramethyldisilane. J Organomet Chem 18:69
39. Zahi I, Mur P, Blaise P, Estève A, Djafari Rouhani M, Vergnes H, Caussat B (2001) Multi-scale modelling of silicon nanocrystal synthesis by low pressure chemical vapor deposition. Thin Solid Films 519:7650–7658
40. Walsh R (1981) Bond-dissociation energy values in silicon-containing compounds and some of their implications. Acc Chem Res 14:246–252
41. Salh R (2011) Defect related luminescence in silicon dioxide network: a review in crystalline silicon: properties and uses. In: Basu S (ed). InTech, Open Access Company, Rijeka, Croatia
42. Daldosso N, Das G, Larcheri S, Mariotto G, Dalba G, Pavesi L, Irrera A, Priolo F, Iacona F, Rocca F (2007) Silicon nanocrystal formation in annealed silicon-rich silicon oxide films prepared by plasma enhanced chemical vapor deposition. J Appl Phys 101:113510